A Generalized Approach to the Design of Microwave Oscillators

YONGNAN XUAN AND CHRISTOPHER M. SNOWDEN, MEMBER, IEEE

Abstract—**A new approach to the design of microwave oscillators is presented which allows both frequency and power output to be predicted. The main feature of this technique is that it allows the optimum performance to be obtained from the active device. This is achieved by employing a generalized substitution theorem, which is described and mathematically proven.**

A design example and experimental results are given for a 12-GHz MESFET oscillator. The experimental results were found to be within 9 percent of the predicted values for both frequency and power, without any experimental adjustment adjustment.

I. Introduction

A NUMBER OF techniques are available for the design of oscillators [1]–[10], [16]–[19]. Generally speaking, the design consists of two parts, namely, the characterization of the active device and the determination of the embedding elements. It is difficult to characterize the active device due to its nonlinear behavior under large-signal conditions associated with oscillators. Oscillators design techniques have been developed using equivalent circuit models for the active device incorporating nonlinear elements, or physical models based on numerical solutions [6], [7], [14], [15], [19]. The former approach is easy to implement and analyze but is generally limited in its applicability because of the frequency dependence and the nonlinear behavior of device characteristics as a function of RF signal level. In contrast, physical models based on numerical simulations can provide greater insight into the detailed operation of the device, encompassing a wide range of operating conditions but requiring a lengthy analysis.

Mitsui *et al.* developed a GaAs MESFET oscillator design method using large-signal *S*-parameters [3]. By dividing the MESFET equivalent circuit elements into two groups, i.e., those which vary significantly under large-signal conditions and those which do not, Johnson proposed another design technique [4]. Since *S*-parameters are dependent on power levels and bias conditions, these techniques are not flexible for varied conditions. An experimental technique for the large-signal characterization of two-port nonlinear active networks was described by Yang and Peterson [24], who used a two-port approach to design a microwave oscillator. A flexible and accurate method was derived by Snowden *et al.* which employed large-signal physical modeling techniques and was used to characterize advice devices and oscillators [12], [14]. A recent development reported by Abe [23] describes a new, quasi-linear approach using small-signal *S*-parameters and static characteristics of FET's to predict oscillation power. By expressing the generated power as a function of intrinsic FET gate and drain RF voltages, the method can be used to maximize the power under limiting conditions for intrinsic FET terminal voltage amplitudes.

In the following sections, a new generalized two-port method and the associated theory are proposed. The method overcomes the difficulties associated with one-port techniques, where the passive elements connected to the active device to obtain a negative-impedance one-port are often chosen empirically, which constrains the design and sometimes makes the prespecification of parameters, such as the power, impossible. In Section II, a generalized substitution theorem is proven which provides the theoretical basis of the oscillator design method. The method itself is described in detail in Section III, while design examples are given in Section IV.

II. A Generalized Substitution Theorem

In this section, a generalized theorem of substitution together with its proofs is given which is used to establish the design method presented in the following section.

Suppose the network N in Fig. 1(a) is a p-port containing active devices and generating positive power. It has port voltages and currents V_j and I_j, respectively, where $j=1,2,\cdots,p$. The state of N will not change when a passive linear p-port N' (Fig. 1(b)) is connected to it if the port impedance matrix Z' of N′ satisfies

$$Z'\bar{I}'_p=\bar{V}'_p$$

where

$$\bar{I}_p=\left[I_1\ I_2\cdots I_p\right]^T \qquad \bar{V}_p=\left[V_1\ V_2\cdots V_p\right]^T$$

and $i=0,1,\cdots,K$ represents ith harmonics.

Starting with the simple case of a one-port circuit, with only a fundamental frequency component, as shown in Fig. 2, and denoting the port loop of N in Fig. 2(a) as the first one, the loop equations of N can be written using Kirchhoff's law as

$$\sum_{j=1}^{L} Z_{ij}J_j=U_i \qquad \text{for } i=1,2,\cdots,L \tag{1}$$

Manuscript received March 9, 1987; revised August 27, 1987.

The authors are with the Microwave Solid-State Group, Department of Electrical and Electronic Engineering, University of Leeds, Leeds LS2 9JT, Great Britain.

IEEE Log Number 8717684.

0018-9480/87/1200-1340$01.00

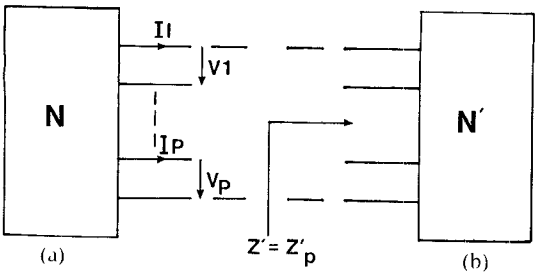

Fig. 1 Substitution of sources with a linear passive network N'.

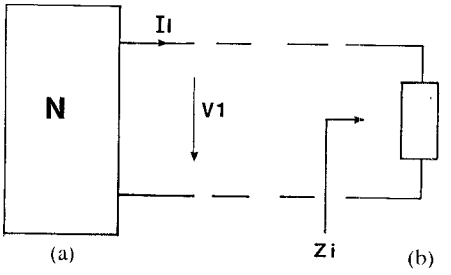

Fig. 2. Special case of Fig. 1 when $p=1$.

where U_i, J_j are loop voltage sources and loop currents, respectively, and

$$Z_{ij}=\begin{cases}\text{loop impedance of the } i\text{th loop for } i=j\\ \text{impedance associated with both } i\text{th and } j\text{th}\\ \quad\text{loops for } i\neq j.\end{cases}$$

L is the number of independent loops of the network N.

Considering the port loop, i.e., the first loop of N, explicitly and noting that $J_1=I_1$, we have

$$\sum_{j=2}^{L} Z_{ij}J_j+Z_{i1}I_1=U_i \qquad \text{for } i=1,2,\cdots,L. \tag{2}$$

Now for the circuit of Fig. 2(b), where the port voltage V_1 has been replaced by a passive impedance branch Z_t which satisfies

$$Z_tI_1=V_1 \tag{3}$$

we can obtain an equation similar to (2). Notice that since Z_t is exclusively in the first loop and not associated with any other loop, it will add a term Z_t only to Z_{i1} without affecting Z_{ij}, for $j=2,3,\cdots,L$. In contrast, the voltage source term V_1 must be deduced from U_1, which describes the first loop voltage sources of network N in Fig. 2(a). Hence,

$$\sum_{j=2}^{L} Z_{ij}J_j+(Z_{i1}+Z_1)I_1=U_1' \qquad \text{for } i=1,2,\cdots,L \tag{4}$$

where Z_{ij} has the same interpretation as that of (2) and

$$U_i'=\begin{cases}U_i \text{ in (2)} & \text{for } i\neq 1\\ U_1 \text{ in (2)}-V_1 & \text{for } i=1.\end{cases}$$

Now by simply inserting (3) into (4) and comparing the result with (2), we find that they are equivalent. This means that the state of the network N in Fig. 2(a) does not change when V_1 is replaced by Z_1 satisfying (3); hence the theorem is correct for this special case.

Considering the more general case shown in Fig. 1(a) and assuming that only signals with a fundamental frequency component are present, the port voltage sources of the network N are replaced by a linear passive p-port N' as shown in Fig. 1(b) with

$$Z_p'\bar{I}_p=\bar{V}_p \tag{5}$$

where Z_p', $\bar{I}_p$, and $\bar{V}_p$ are the impedance matrix, port current vector, and port voltage vector, respectively.

For simplicity, we will give the mathematical proof for this case in matrix form. For the circuit shown in Fig. 1(a), the loop equations can be expressed as

$$\begin{bmatrix}Z_p & Z_{NP}\\ Z_{PN} & Z_N\end{bmatrix}\begin{bmatrix}\bar{J}_p\\ \bar{J}_N\end{bmatrix}=\begin{bmatrix}\bar{U}_p\\ \bar{U}_N\end{bmatrix} \tag{6}$$

where the subscript p indicates the loops containing port branches; $\bar{U}_p$ and $\bar{J}_p$ are the voltage source and the current of such loops, respectively; and Z_{NP}, Z_{pN}, Z_N, $\bar{J}_N$, and $\bar{U}_N$ are submatrices or vectors of the inner loops of N.

On the other hand, following a manipulation procedure similar to the one for the circuit shown in Fig. 2(b) and noting that the submatrix Z_p' in (5) does not affect Z_{NP}, Z_{pN}, and Z_N but only Z_p, the loop equations for the circuit shown in Fig. 1(b) will appear as

$$\begin{bmatrix}Z_p+Z_p' & Z_{NP}\\ Z_{pN} & Z_N\end{bmatrix}\begin{bmatrix}\bar{J}_p\\ \bar{J}_N\end{bmatrix}=\begin{bmatrix}\bar{U}_p'\\ \bar{U}_N\end{bmatrix} \tag{7}$$

where vector $\bar{U}_p'$ is the difference between $\bar{U}_p$ and $\bar{V}_p=[V_1\ \ V_2\ \ \cdots\ \ V_p]^T$ for the circuit shown in Fig. 1(a), because of the substitution of the port voltage sources by the linear passive p-port N'. Inserting (5) into (7) and comparing the result with (6), it can be seen that for the loops containing port branches $\bar{I}_p=\bar{J}_p$, the circuits shown in Fig. 1 are equivalent since they have the same loop equations, if we consider only the state of the network N.

Finally, in the circumstances where the signals contain harmonic components in addition to the fundamental frequency, we can prove that the theorem remains valid by considering the circuits shown in Fig. 1 again, with harmonic frequencies taken into account. Since the existence of harmonics does not change the topology of both circuits, we are assured that the loop equations in this case will have the same appearance as (5), (6), and (7) with all the elements being functions of frequency. Due to the periodicity of the signals dealt with, the branch voltages and currents of the circuits can be expressed as

$$i(t)=\mathrm{Re}\sum_{l=1}^{K} I^l e^{jl\omega t} \tag{8}$$

$$u(t)=\mathrm{Re}\sum_{l=1}^{K} U^l e^{jl\omega t} \tag{9}$$

where K is the number of harmonics of significance, and

the coefficients for ith harmonics are

$$I^i = \frac{1}{2\pi}\int_{-\pi}^{\pi} i(t)e^{-ji\omega t}\,dt \tag{10}$$

$$U^i = \frac{1}{2\pi}\int_{-\pi}^{\pi} u(t)e^{-ji\omega t}\,dt. \tag{11}$$

On the other hand, the harmonic-balance constraint of the linear circuit gives the following relationship in the frequency domain:

$$Z(i\omega)\overline{I^i} = \overline{U^i}. \tag{12}$$

This confirms that the conclusion given for the fundamental-frequency-only case is valid for every harmonic and therefore the proof of the generalized theorem is complete.

III. Oscillator Design Procedure

An oscillator consists of an active device and a passive load, which may be viewed as the embedding circuit for the active device. The aim here is to design the embedding circuit for a specific active device so that the resulting oscillator operates to the required specifications while obtaining the optimum performance from the active device. In order to achieve the optimum device–circuit interaction, the characteristics of the embedding circuit and the interactions between it and the device should be carefully investigated. The characteristics of embedding circuits can be divided into two categories, those forming terminating impedances for both the input and the output and those providing feedback paths, which are required for oscillators using three-terminal active devices. In order to optimize the performance of the oscillator, it is hoped that the whole embedding circuit can be determined simultaneously.

The basic philosophy of the present design technique presented here is to match the passive embedding elements to the conditions required for optimal operation of the active device. This means that the limitations on the performance of the MESFET caused by the arbitrary connection of some or all of the embedding elements are reduced to a minimum.

The embedding circuit design technique is outlined in the following basic steps:

(a) Taking the active device without embedding elements connected to it as a two port N, apply two voltage sources, $U_1(t)$ and $U_2(t)$, to port I and port II, respectively, and obtain the current responses in each port (namely $i_1(t)$ and $i_2(t)$). The variables in the time domain are transformed into corresponding ones in the frequency domain so that U_1^i, U_2^i, I_1^i, and I_2^i are obtained, where $i = 0,1,2,\cdots,K$ represents the variables at the ith harmonic, and K is the number of harmonics of significance. Optimization, if required, should be performed in this stage.

(b) Using the optimized U_1^i, U_2^i, I_1^i, and I_2^i as the port variables, the passive embedding two-port network N′ is synthesized (Fig. 3).

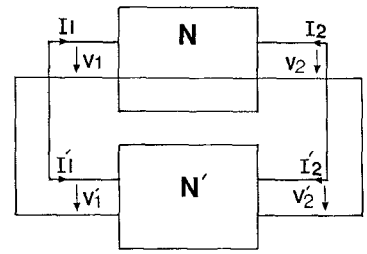

Fig. 3. Interconnection of the device N and the passive embedding network N′.

The importance of applying two signal sources to characterize the isolated device should be noted. The fact that there is no constraint placed on the voltages and currents associated with the sources guarantees that the results obtained in the characterization are determined only by the properties of the device itself. In this way, the optimization to obtain maximum power output at a given frequency reflects the full potential of the active device.

Step (a) can be carried out by using equivalent circuit models, physical modeling techniques, or other techniques based on measurements. The details of the physical modeling technique, developed by one of the authors, which has been used in the oscillator design can be found in [11], [12], and [14] and will not be described in detail here. Another technique for the characterization of the MESFET at microwave frequencies based on S-parameters may also be used to obtain the port voltages and port currents mentioned in step (a). The S-parameters of the device used were measured and transformed into an admittance matrix Y_d which describes explicitly the relationships between the voltages and currents in the input and output ports of the MESFET.

Two voltages, U_1, and U_2, are superimposed and used together with Y_d to calculate the currents I_1 and I_2. It should be noticed that for optimal and stable oscillations to be obtained, U_1 and U_2 have to be carefully optimized. The key parameters are the amplitudes of the two voltages and the phase difference between them; these parameters substantially affect not only the characterization of the device in step (a), but also the calculation of the embedding elements in step (b), as will be discussed later in this section. Since it is the saturated properties of the device which determine the characteristics of the steady state of oscillations obtainable and since that signal level has a large effect on the gain properties of the FET [21], we chose the parameters mentioned above with the following considerations. The dc characteristics of the device were referred to in determining the approximate varied range of the amplitudes of U_1 and U_2 in the optimization to obtain maximum output power [7], [23]. On the other hand, since the frequency of the oscillation is determined mainly by the passive network [21], higher frequency selectivity from the input port to the output port of the passive network is desirable. We took this as another criterion in choosing the phase difference between U_1 and U_2, and a suitable value was chosen, so that the value of Q of the passive network (the transfer impedance) was as high as possible ($\gg 10$) in

order to achieve oscillations at the specified frequency. Different emphasis can be attached to the power output and the frequency selectivity to meet different requirements of the design. Since S-parameters of devices are dependent on signal levels, it is important to note that the port voltages and currents are meaningful only if they are obtained at the same power level as that at which the S-parameters were measured or computed. Errors will be inevitable to some extent if this is not satisfied. Techniques of computing and measuring large-signal S-parameters are discussed in [4].

The constraints on the second part of the procedure (step (b)) will now be discussed. Since the device is in general a nonreciprocal element, Y_d is consequently a nonsymmetric matrix, i.e., $Y_{12} \neq Y_{21}$. So it is impossible to obtain the admittance matrix Y of the embedding circuit by simply equating the corresponding elements of them, because Y is symmetric due to the passivity of the embedding circuit. Reference to Fig. 3 shows that by placing the terminals of the device in different positions, there are several possible configurations which can be obtained. But for any configuration, the relationships given by the following two equations are always automatically satisfied:

$$U_1^i = U_1'^i \tag{13}$$

$$U_2^i = U_2'^i. \tag{14}$$

The conditions for equilibrium oscillations are

$$I_1^i + I_1'^i = 0 \tag{15}$$

$$I_2^i + I_2'^i = 0 \tag{16}$$

where U_1^i, U_2^i, I_1^i, and I_2^i are obtained in step (a).

From (13)–(16),

$$I_1^i + f_1^i(U_1^i, U_2^i, X, T) = 0 \tag{17}$$

$$I_2^i + f_2^i(U_1^i, U_2^i, X, T) = 0 \tag{18}$$

where X is a set of element parameters of N′, T is the topology of N′, f_1^i and f_2^i are linear functions of U_1^i, U_2^i, and T, $i = 0, 1, 2, \cdots, K$ with its meaning given previously.

Notice that (17) and (18) are in a generalized form and are valid for any kind of topology of the embedding circuit and interconnections between embedding circuit and active device. This provides us with the flexibility of choosing configurations while taking other factors, for example economy and realizability, into account in the design of the circuit. The two simplest topologies of N′ are the Π and T types, shown in Fig. 4(a) and (b), respectively. This allows series or parallel tuned circuits to be incorporated into the network as part of the embedding network.

As soon as the topology T in (17) and (18) is chosen, the equations can be written explicitly and the circuit element can be readily obtained by solving the resulting equations. For example, in the case of the Π configuration, shown in Fig. 4(a), (17) and (18) become

$$I_1 + U_1 Y_1 + (U_1 - U_2) Y_3 = 0 \tag{19}$$

$$I_2 + U_2 Y_2 + (U_2 - U_1) Y_3 = 0. \tag{20}$$

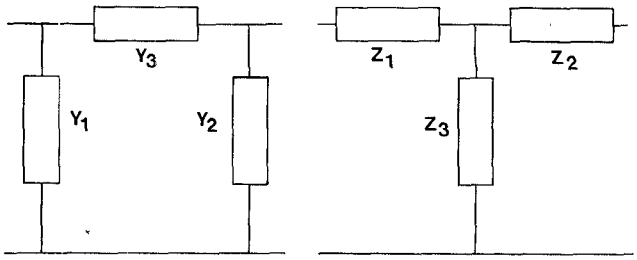

Fig. 4. Two special cases of the embedding network N′: Π and T networks.

Here for the sake of simplicity, only the fundamental frequency is considered.

Note that the current and voltage variables in these two equations are known from step (a) of the design procedure. Equations (19) and (20) are solved to obtain the admittances of the elements in N′, namely, Y_1, Y_2, and Y_3.

For the admittances

$$Y_m = G_m + jB_m, \qquad m = 1, 2, 3 \tag{21}$$

by inserting (21) into (19) and (20) and equating the real and imaginary parts of each equation to zero, respectively, we obtain

$$\begin{aligned}
&I_{1R} + U_{1R}G_1 - U_{1I}B_1 \\
&\qquad + (U_{1R} - U_{2R})G_3 - (U_{1I} - U_{2I})B_3 = 0 \\
&I_{1I} + U_{1I}G_1 + U_{1R}B_1 \\
&\qquad + (U_{1R} - U_{2R})B_3 + (U_{1I} - U_{2I})G_3 = 0 \\
&I_{2R} + U_{2R}G_2 - U_{2I}B_2 \\
&\qquad + (U_{2R} - U_{1R})G_3 - (U_{2I} - U_{1I})G_3 = 0 \\
&I_{2I} + U_{2I}G_2 + U_{2R}B_2 \\
&\qquad + (U_{2R} - U_{1R})B_3 + (U_{2I} - U_{1I})G_3 = 0.
\end{aligned} \tag{22}$$

Here we have four equations with the six unknown variables G_m and B_m, $m = 1, 2, 3$, two of which, say G_1 and G_2, can be chosen while the remaining four are to be found from (21).

In this way, (21) becomes

$$\begin{bmatrix}
U_{1R} - U_{2R} & -U_{1I} & 0 & -U_{1I} + U_{2I} \\
U_{1I} - U_{2I} & U_{1R} & 0 & U_{1R} - U_{2R} \\
U_{2R} - U_{1R} & 0 & -U_{2I} & U_{1I} - U_{2I} \\
U_{2I} - U_{1I} & 0 & U_{2R} & -U_{1R} + U_{2R}
\end{bmatrix}
\begin{bmatrix} G_3 \\ B_1 \\ B_2 \\ B_3 \end{bmatrix}$$

$$= -\begin{bmatrix}
I_1 R + U_1 R G_1 \\
I_1 I + U_1 I G_1 \\
I_2 R + U_2 R G_2 \\
I_2 I + U_2 I G_2
\end{bmatrix}. \tag{23}$$

This equation can be solved relatively easily, but there are several important points to note. First, for the embedding network to be realized with passive elements, G_3 must be positive. This can be guaranteed so long as the net output power obtained in step (a) is positive, which should be ensured when carrying out this step. Second, the independent voltage sources $U_1(t)$ and $U_2(t)$ applied to port I and port II should have different phases. This is achieved as

follows. Denoting the coefficient matrix on the left-hand side of (22) as C, the following condition should be satisfied:

$$|C| \neq 0 \tag{24}$$

where $|C|$ is the determinant of the matrix C.

Through simple manipulations of (23) and (24), we have

$$(U_{1R}U_{2I} - U_{1I}U_{2R})\left[(U_{1R} - U_{2R})^2 + (U_{1I} - U_{2I})^2\right] \neq 0. \tag{25}$$

This is equivalent to

$$U_1 \neq 0$$

$$U_{1R}U_{2I} - U_{1I}U_{2R} \neq 0.$$

Or we can obtain from the above two inequalities

$$\frac{U_{1R}}{U_{1I}} \neq \frac{U_{2R}}{U_{2I}} \tag{26}$$

i.e., for (23) to have a meaningful solution, there must be a phase difference between $U_1(t)$ and $U_2(t)$. At this stage $U_1(t)$, $U_2(t)$ and their associated phases, which describe the state of the device, are chosen and adjusted in order to optimize the values of I_1 and I_2 to obtain maximum output power.

Third, the coefficient matrix C could be very ill conditioned due to the intrinsic properties of the active device. For instance, for a MESFET circuit in common-source configuration, the elements in the second column of C could be very small compared with some other elements in the matrix. To overcome this difficulty, scaling of some columns or rows of the matrix is sometimes necessary.

Another possible problem is that the diagonal element (3.3) in C may be too small, which adversely affects the conditions of the matrix to a considerable extent. This problem arises in cases where the phase angle of U_2 is close to 180°. Since the phase of U_1 is not constrained to follow any phase changes in U_2 during the optimization, the initial choice of U_2 phase angle influences the solution. Notice that it is the phase difference between U_1 and U_2, rather than the absolute phases of the individual voltages, which affects the design of the embedding network. Hence, in general, this difficulty can be resolved by defining a suitable phase of U_1 so that the phase of U_2, which is itself determined by that of U_1, and the characteristics of the device are around 30° away from 180°.

Finally, it is interesting to make a comparison between the new method and the well-established negative-resistance one-port design approach [1], [3], [5]. The two techniques are in principle very similar from the viewpoint that they both use an embedding circuit (or a load) with appropriate characteristics to replace the signal sources impressed on the device during the design process and simulation. On the other hand, there are several important differences. As mentioned in Section I, in addition to the fact that the "device surface" and the "load locus" of the one-port method [3], [5] are generalized in a multidimensional space, the use of two signal sources in device characterization and the fact that no element is chosen empirically make this approach an optimal design in the true sense.

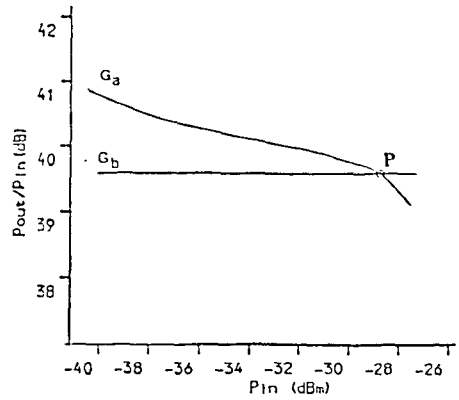

Fig. 5. Variation of power gain with input power for the low-frequency BJT oscillator. P is the chosen operating point

IV. Experimental Results

Two oscillators were fabricated using this proposed design method. One of them is a low-frequency design at 10 kHz using a silicon bipolar transistor. The other operates at J-band using a 0.5-μm-gate-length MESFET mounted on microstrip substrate.

In the case of the bipolar transistor used in the 10-kHz oscillator, the power-gain characteristic measured while two voltage sources were applied to its base–emitter and collector–emitter ports, respectively, is shown in Fig. 5 as curve G_a. Curve G_b in the figure shows the ratio of the power flowing into port 2 of the embedding network and that out of port 1 and fed back to the transistor. The ratio is constant because of the linearity of the passive elements. P is chosen as the operating point where saturation begins and the harmonics content of the signal is small.

The relationship between G_a and G_b assures us that oscillations can build up and will become stable at P. These can be seen by noting that for $P_{\text{in}} < P'_{\text{in}}$, G_a is always greater than G_b, which means that the power fed back to the input port of the device through the embedding circuit is more than that required for stable oscillation. So the oscillations will be getting larger and larger until point P is reached. Since at this point,

$$G_a = G_b$$

and

$$\frac{\partial Ga}{\partial P_{\text{in}}} < \frac{\partial Gb}{\partial P_{\text{in}}} \qquad \frac{\partial Gb}{\partial P_{\text{in}}} = 0$$

the oscillations will remain stable.

The circuit obtained is shown in Fig. 6. The frequency and power measured are 9.26 kHz and 10.2 mW, respectively, compared with 10 kHz and 12.1 mW obtained from the design process. The errors in these results appear to be mainly due to the parasitics of the embedding elements used in the circuit. In particular, it was found that the coil resistance of the inductor accounted for a large part of the discrepancy.

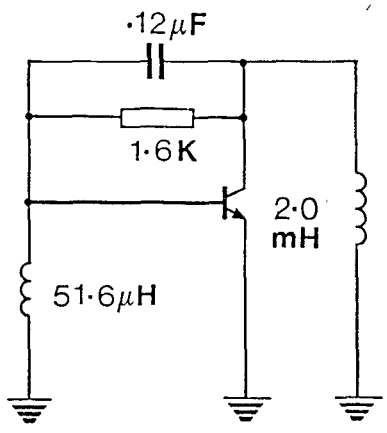

Fig. 6. Circuit diagram of the low-frequency BJT oscillator.

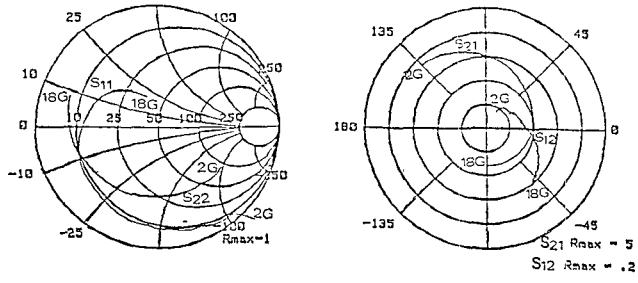

Fig. 7. Measured S parameters of the NE700 MESFET.

TABLE I
MEASURED S-PARAMETERS AT 12 GHz FOR NE700

	Re	Im	AMPL	PHASE
S_{11}	-.653	0.09	.660	172.3
S_{21}	1.534	.232	1.55	-8.6
S_{12}	.066	.023	.070	-19.45
S_{22}	-.527	.419	.673	-142.2

The microwave oscillator was fabricated using a NE700 MESFET. The measured S-parameter characteristics of the device are shown in Fig. 7. The S-parameters at the frequency of 12 GHz are shown in Table I. The amplitude of S_{12}, the reverse transmission parameter which is known to reduce the stability of the device, is found to be less than 0.075 up to the frequency of 13.5 GHz and is 0.07 at 12 GHz. The S parameters were measured under the bias conditions of $V_{DS} = 3$ V and $I_D = 30$ mA, which are the ones used in circuit design.

The characterization of the MESFET and the optimization of the oscillator circuit design were carried out using the techniques described in Section III. Although in principle a variety of models are suitable for use in this analysis and design, the measured S parameters shown in Fig. 7 were used in the design example. In accordance with the design equations in Section III, two independent voltages were imposed on the input and output ports of the model and the resulting currents calculated. With reference to Fig. 3, the power output from the device can be expressed as

$$P_{\text{out}} = -R_e(U_1 I_1^* + U_2 I_2^*).$$

Since I_1 and I_2 are determined by U_1, U_2, and the characteristics of the device, it can be seen from the above equation that, for a given device, P_{out} is a function of U_1 and U_2. The amplitudes and phases of these voltages (U_1 and U_2) were changed in order to optimize the circuit to obtain maximum power output from the device. The optimization was carried out by fixing three of the four parameters (the amplitudes and phases of U_1 and U_2) and changing the fourth parameter to obtain an increase of P_{out}. This process was repeated for each of the amplitudes and phases of U_1 and U_2 until P_{out} reached the maximum value obtainable from the device. The optimization is an iterative procedure, and the initial choice of U_1 and U_2 has a significant effect on the number of iterations required and the accuracy of the numerical calculations. It was found that the dc characteristics provided a useful set of initial conditions, assuming that the device operates in the saturation region (the guidelines proposed in Section III were followed when selecting the phase of U_1 and U_2). A set of initial and optimized values of the voltages and currents is listed in Table II. After obtaining U_1, U_2, I_1, and I_2 from the optimization routine, the embedding circuit was synthesized using these parameters as port variables according to (17) and (18). The actual forms of the equations used depend on the specific topologies chosen for the circuit, but are available in most network theory texts. In the case of the Π configuration, the network equations take the same form as (22), with U_1, U_2, I_1, and I_2 as the known parameters and the G's and B's as the unknown circuit element parameters. Several topologies were investigated for use in this design. The Π configuration was chosen because the element values obtained with it can be more easily implemented using microstrip techniques.

TABLE II
INITIAL AND OPTIMIZED VALUES OF VOLTAGES AND CURRENTS

	Initial	Optimized
$V_1(mV)$	110-j12	131-j9.8
$V_2(mV)$	-1050+j300	-1278+j328
$I_1(mA)$	0.518+j4.75	0.420+j5.7
$I_2(mA)$	-10.87-j11.43	-13.2-j14.4

The final circuit is shown in Fig. 8. Careful consideration was also given to the layout of the microstrip to minimize parasitic effects due to the discontinuities and

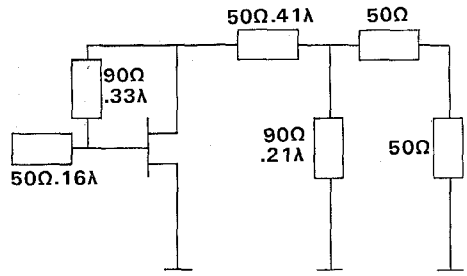

Fig. 8. Circuit diagram of the microwave FET oscillator.

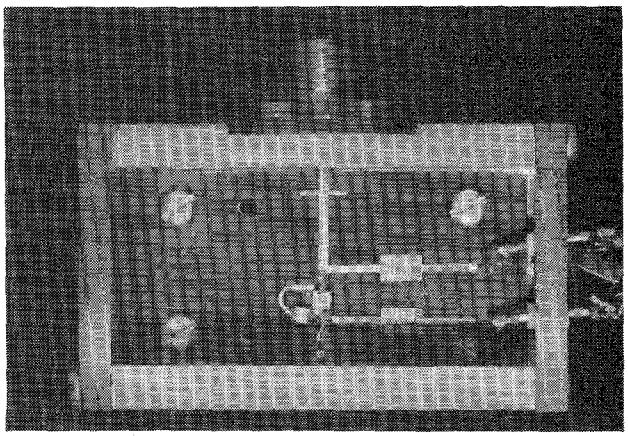

Fig. 9. Photograph of the fabricated oscillator.

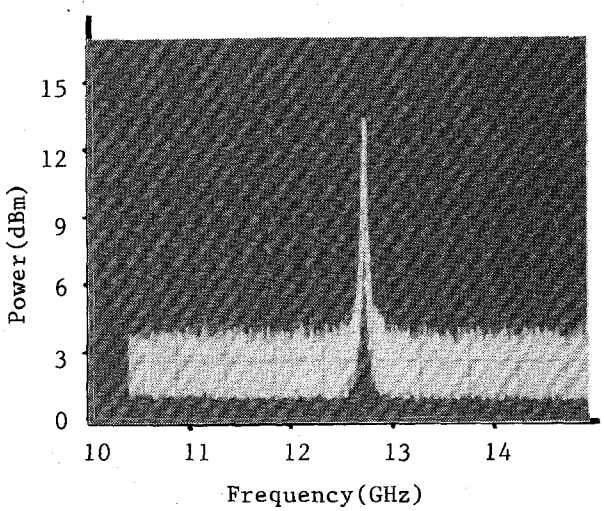

Fig. 10. Spectrum of the microwave FET oscillator.

spurious couplings. For example, a semicircular loop of microstrip line was used in the section between the gate and the drain of the MESFET which acts as an inductor to reduce the effect of the parasitic capacitance associated with right-angle corners. RT-Duroid substrate was used with a thickness of 0.254 mm and a relative dielectric constant ϵ_r of 2.2. Shown in Fig. 9 is a photograph of the microwave oscillator fabricated.

The measured power output and frequency were 23.7 mW and 12.7 GHz, compared with the predicted values of 21.6 mW and 12 GHz, respectively. The efficiency was measured at 24 percent, compared to the 22 percent predicted. The measured spectrum of the oscillator is shown in Fig. 10. It should be noted that no empirical adjustment was carried out prior to obtaining these measurements.

V. Conclusions

A new generalized substitution theorem and its mathematical proof are presented for the first time. An efficient oscillator design approach based on this theorem is described. The method allows the frequency to be accurately determined and the power output of the oscillator to be optimized. Both mathematical and physical aspects of the embedding circuit design are discussed. The method has been verified for several practical designs, of which two design examples and measured results are given. Very good agreement between the predicted and measured results has been obtained.

References

[1] K. Kurokawa, "Some basic characteristics of broadband negative resistance oscillator circuits," *Bell Syst. Tech. J.*, vol. 48, pp. 1937–1955, July 1969.

[2] M. Maeda *et al.*, "Design and performance of *X*-band oscillators with GaAs Schottky-gate field-effect transistors," *IEEE Trans. Microwave Theory Tech.*, vol. MTT-23, pp. 661–667, Aug. 1975.

[3] Y. Mitsui *et al.*, "Design of GaAs MESFET oscillator using large signal *S*-parameters," *IEEE Trans. Microwave Theory Tech.*, vol. MTT-22, pp. 981–984, Dec. 1977.

[4] K. M. Johnson, "Large signal GaAs MESFET oscillator design," *IEEE Trans. Microwave Theory Tech.*, vol. MTT-27, pp. 217–227, Mar. 1979.

[5] G. R. Basawapatna *et al.*, "A unified approach to the design of wide band microwave solid-state oscillators," *IEEE Trans. Microwave Theory Tech.*, vol. MTT-27, pp. 379–385, May 1979.

[6] C. Rauscher, "Optimum large-signal design of fixed-frequency and varactor-tuned GaAs FET oscillators," in *IEEE MTT-S Int. Microwave Symp. Dig.*, 1980, pp. 373–375.

[7] Y. Tazima *et al.*, "GaAs FET large-signal model and its application to circuit designs," *IEEE Trans. Electron Devices*, vol. ED-28, pp. 171–175, Feb. 1981.

[8] D. J. Esdale *et al.*, "A reflection coefficient approach to the design of one-port negative impedance oscillators," *IEEE Trans. Microwave Theory Tech.*, vol. MTT-29, pp. 770–776, Aug. 1981.

[9] Y. Yukang *et al.*, "Monolithic microwave integrated GaAs FET oscillators," in *IEEE MTT-S Int. Microwave Symp. Dig.*, 1982, pp. 289–290.

[10] V. Rizzoli *et al.*, "A computer-aided approach to the nonlinear design of microwave transistor oscillators," in *1982 IEEE MTT-S Dig.*, pp. 453–455.

[11] C. M. Snowden, "Numerical simulation of microwave GaAs MESFETs," in *Proc. Int. Conf. Simulation of Semiconductor Devices and Processes* (Swansea, U.K.), July 1984, pp. 406–425.

[12] C. M. Snowden *et al.*, "Microwave FET oscillator design based on large-signal characterisation," in *Proc. 13th European Microwave Conf.*, Sept. 1983, pp. 623–627.

[13] M. J. Howes *et al.*, "Large-signal characterisation plus computer graphics aid oscillator design," *Microwave Syst. News*, pp. 42–57, Oct. 1979.

[14] C. M. Snowden, M. J. Howes, and D. V. Morgan, "Large-signal modeling of GaAs MESFET operation," *IEEE Trans. Electron Devices*, vol. ED-30, pp. 1817–1824, Dec. 1983.

[15] R. E. Bank, "Numerical methods for semiconductor device simulation," *SIAM Sci. Stat. Comput.*, vol. 4, no. 3, pp. 416–435, Sept. 1983.

[16] R. J. Trew, "Design theory for broad-band YIG-tuned FET oscillators," *IEEE Trans. Microwave Theory Tech.*, vol. MTT-27, pp. 8–14, Jan. 1979.

[17] R. J. Gailmore *et al.*, "GaAs MESFET oscillator design using large-signal *S*-parameters," in *IEEE MTT-S Int. Microwave Symp. Dig.*, 1983, pp. 279–281.

[18] E. R. Ehlers, "An empirical design technique for microwave oscillators," *IEEE Trans. Microwave Theory Tech.*, vol. MTT-32, pp.

556–559, May 1984.
[19] W. R. Curtice, "A nonlinear GaAs FET model for use in the design of output circuit for power amplifier," *IEEE MTT-S Int. Microwave Symp. Dig.*, 1985, pp. 405–408.
[20] *S-Parameter Techniques for Faster, More Accurate Network Design*, Hewlett-Packard Application Note 95-1, pp. 1–12.
[21] H. J. Reich, *Functional Circuits and Oscillators*. New York: Van Nostrand, 1961.
[22] W. R. Curtice, "Self-consisted GaAs FET model for amplifier design and device diagnostics," *IEEE Trans. Microwave Theory Tech.*, vol. MTT-32, pp. 1573–1578, Dec. 1984.
[23] H. Abe, "A GaAs MESFET oscillator quasi-linear design method," *IEEE Trans. Microwave Theory Tech.*, vol. MTT-34, pp. 19–25, Jan. 1986.
[24] D. C. Yang and D. F. Peterson, "Large-signal characterisation of two-port non-linear active networks," in *Proc. IEEE MTT-S* (Dallas, TX), 1982, pp. 345–347.

✠

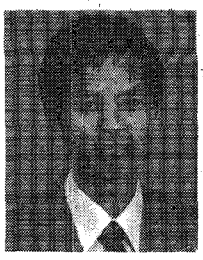

Xuan Yongnan was born in Guangazhou, China, on March 10, 1953. He received the B.Sc. degree from the South China Institute of Technology (SCIT) in 1982.

He was a teacher at the SCIT from January 1982 to October 1985. In October 1985 he joined the Department of Electrical and Electronic Engineering at the University of Leeds, England, as a visiting researcher. He is now a postgraduate student in the department. His research interests are modeling of active and passive components and CAD design of monolithic integrated circuits.

✠

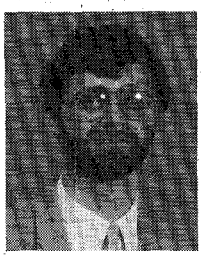

Christopher M. Snowden (M'82) was born in Hull, England, on March 5, 1956. He received the B.Sc., M.Sc., and Ph.D. degrees from the University of Leeds, Leeds, England. His Ph.D. studies were conducted in association with Racal-MESL, and were concerned with large-signal characterization of MESFET oscillators.

After graduating, he worked as an Applications Engineer for Mullard, Mitcham. In 1982, he was appointed a Lecturer in the Department of Electronics at the University of York. Since July 1983, he has been a Lecturer in the Microwave Solid State Group in the Department of Electrical and Electronic Engineering at the University of Leeds. His main research interests are concerned with microwave devices, subsystems, and semiconductor device modeling.

Dr. Snowden is a founder member of the International GaAs Simulation Group.